

Supporting Information

Phosphorus-Modified Fe₄N@N, P Co-doped Graphene as Efficient Sulfur Host for High-Performance Lithium-Sulfur Batteries

Meng Zhang,^a Lu Wang,^a Bin Wang,^a Bo Zhang,^a Xiuping Sun,^a Debao Wang,^b Zhen Kong,^a Liqiang Xu*^{a,c}

^aKey Laboratory of Colloid and Interface Chemistry, Ministry of Education, School of Chemistry and Chemical Engineering, Shandong University, Jinan 250100, P. R. China.

^bCollege of Chemistry and Molecular Engineering, Qingdao University of Science and Technology, Qingdao 266042, China

^c Shandong Provincial Key Laboratory/Collaborative Innovation Center of Chemical Energy Storage & Novel Cell Technology, Liaocheng University, Liaocheng City 252059, China

*Corresponding author.

E-mail: xulq@sdu.edu

Content

Figure captions:

- Fig. S1.** TEM and FESEM images of the obtained $\text{Fe}_2\text{O}_3@\text{rGO}$.
- Fig. S2.** (a) TEM, (b) HRTEM and (c-d) FESEM images of the obtained $\text{Fe}_4\text{N}@\text{NG}$.
- Fig. S3.** TEM images of P- $\text{Fe}_4\text{N}@\text{NPG}$ after 1 hour sonication.
- Fig. S4.** (a, b) FESEM images and (c) The corresponding EDS elemental mapping images of the obtained P- $\text{Fe}_4\text{N}@\text{NPG}/\text{S}$ composite.
- Fig. S5.** (a) TEM and (b) FESEM images of NPG. (c) The corresponding EDS elemental mapping of NPG. (d) EDS spectrum and (e) percentage of elements of NPG.
- Fig. S6.** The typical XRD pattern of the obtained $\text{Fe}_2\text{O}_3@\text{rGO}$.
- Fig. S7.** TGA curves of (a) $\text{Fe}_4\text{N}@\text{NG}/\text{S}$ and (b) $\text{Fe}_2\text{O}_3@\text{rGO}/\text{S}$.
- Fig. S8.** Pore size distribution curves of P- $\text{Fe}_4\text{N}@\text{NPG}$ and P- $\text{Fe}_4\text{N}@\text{NPG}/\text{S}$.
- Fig. S9.** XPS spectrum of the Fe 2p in full spectrum of P- $\text{Fe}_4\text{N}@\text{NPG}$ after Li_2S_6 adsorption.
- Fig. S10.** (a, b) Cycling performances of P- $\text{Fe}_4\text{N}@\text{NPG}/\text{S}$ cathode at 0.1 and 0.2 C, respectively. (c) Galvanostatic charge/discharge profiles of the P- $\text{Fe}_4\text{N}@\text{NPG}/\text{S}$ cathode under different current densities. (d) Galvanostatic charge/discharge profiles of P- $\text{Fe}_4\text{N}@\text{NPG}/\text{S}$ cathode at 1 C.
- Fig. S11.** (a) CV curves of P- $\text{Fe}_4\text{N}@\text{NPG}/\text{S}$, $\text{Fe}_4\text{N}@\text{NG}/\text{S}$ and $\text{Fe}_2\text{O}_3@\text{rGO}/\text{S}$ cathodes at scan rate of 0.1 mV s^{-1} . (b) The linear sweep voltammetry scanning curves. (c) Galvanostatic charge/discharge profiles of P- $\text{Fe}_4\text{N}@\text{NPG}/\text{S}$, $\text{Fe}_4\text{N}@\text{NG}/\text{S}$ and $\text{Fe}_2\text{O}_3@\text{rGO}/\text{S}$ cathodes at 0.5 C.
- Fig. S12.** The electrochemical performance of $\text{Fe}_2\text{O}_3@\text{rGO}/\text{S}$ cathode. (a) CV curves of $\text{Fe}_2\text{O}_3@\text{rGO}/\text{S}$ cathode at a scan rate of 0.1 mV s^{-1} . (b) Galvanostatic charge/discharge profiles and (c) Long-term cycling performance of $\text{Fe}_2\text{O}_3@\text{rGO}/\text{S}$ cathode at 1C.
- Fig. S13.** The electrochemical performance of $\text{Fe}_4\text{N}@\text{NG}/\text{S}$ cathode. (a) CV curves of $\text{Fe}_4\text{N}@\text{NG}/\text{S}$ cathode at a scan rate of 0.1 mV s^{-1} . (b) Galvanostatic charge/discharge profiles and (c) Long-term cycling performance of $\text{Fe}_4\text{N}@\text{NG}/\text{S}$ cathode at 1 C.
- Fig. S14.** Long-term cycling performance of P- $\text{Fe}_4\text{N}@\text{NPG}/\text{S}$ cathode at 2 C.
- Fig. S15.** (a) CV curves of NPG/S cathode at a scan rate of 0.1 mV s^{-1} . (b) Cycling performance and coulombic efficiency of NPG/S cathode at 0.2 C. (c) The typical galvanostatic charge/discharge voltage profiles of P- $\text{Fe}_4\text{N}@\text{NPG}/\text{S}$ and NPG/S cathodes at 0.2 C.
- Fig. S16.** (a) The electrochemical impedance spectra (EIS) of P- $\text{Fe}_4\text{N}@\text{NPG}/\text{S}$, $\text{Fe}_4\text{N}@\text{NG}/\text{S}$ and $\text{Fe}_2\text{O}_3@\text{rGO}/\text{S}$ cathodes before cycling. (b) The relationship between the Z' square root of angular frequency ($\omega^{-0.5}$).
- Fig. S17.** (a, b) Coulombic efficiency of P- $\text{Fe}_4\text{N}@\text{NPG}/\text{S}$ cathode of lean electrolyte at 0.2 C and 0.1 C, respectively.
- Fig. S18.** Density of states of P- Fe_4N .
- Table S1.** The electrochemical performance of P- $\text{Fe}_4\text{N}@\text{NPG}/\text{S}$ in this work compared with other similar materials reported in lithium-sulfur batteries.

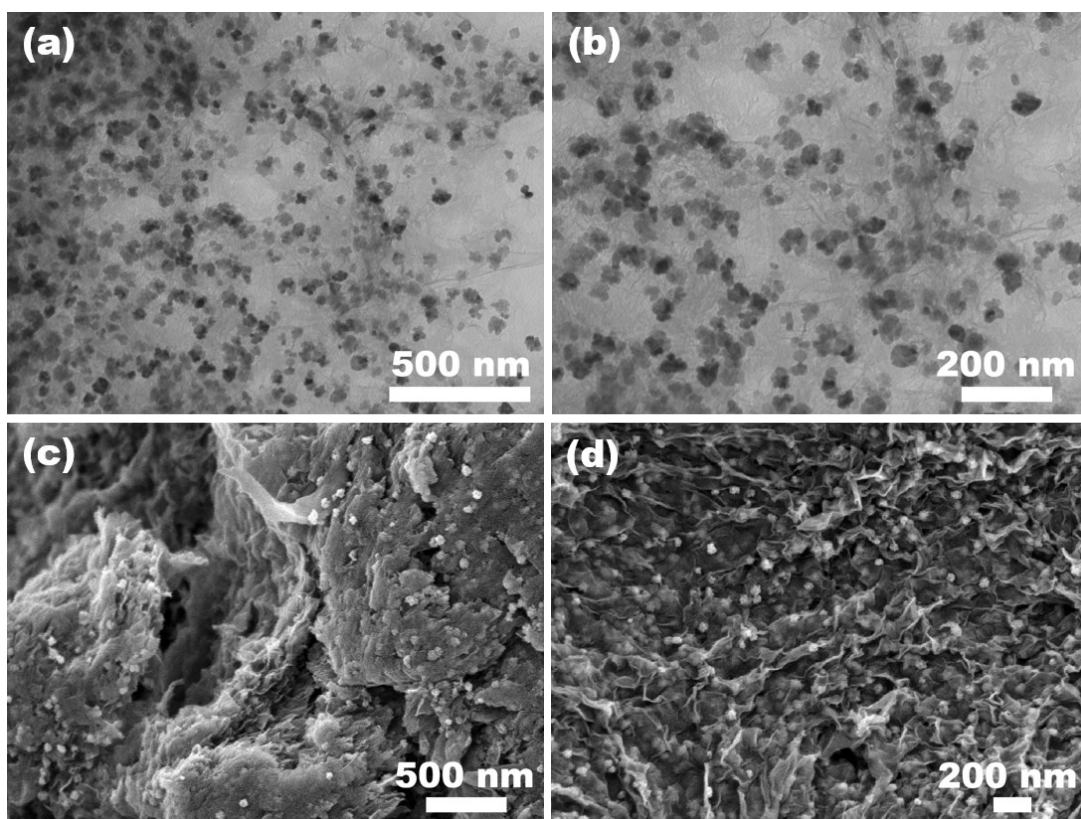


Fig. S1. TEM and FESEM images of the obtained $\text{Fe}_2\text{O}_3@\text{rGO}$.

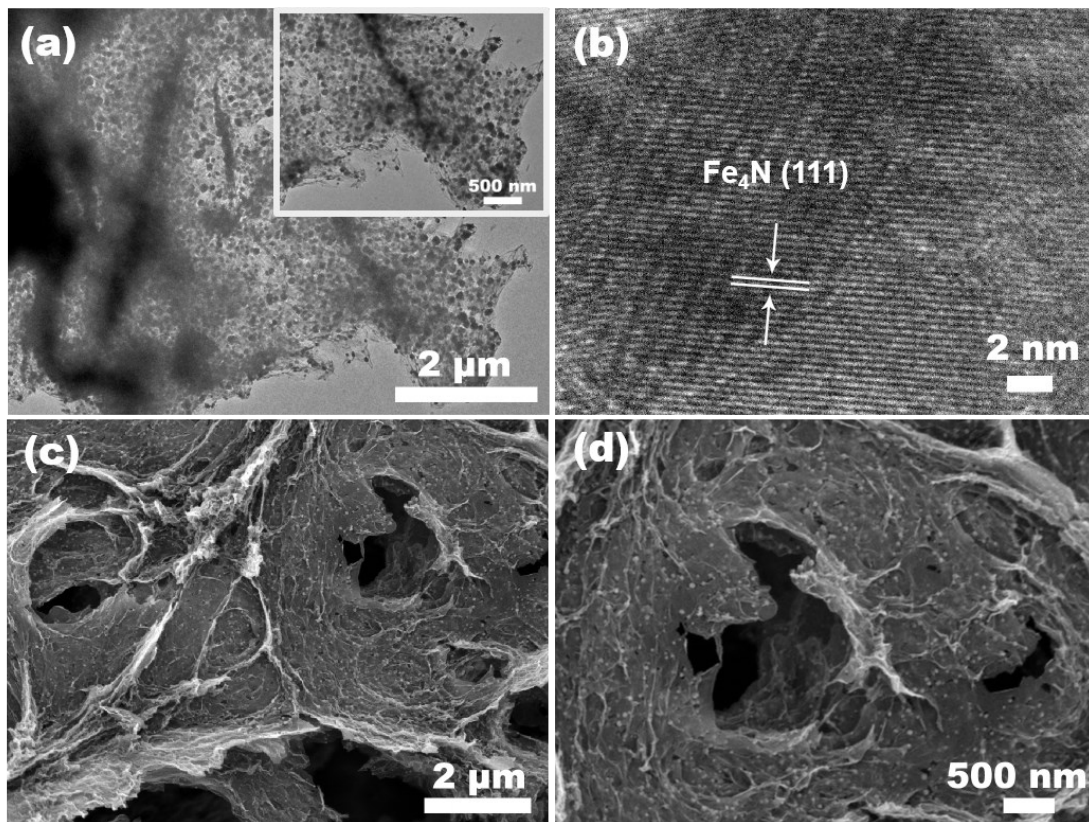


Fig. S2. (a)TEM, (b) HRTEM and (c-d) FESEM images of the obtained Fe₄N@NG.

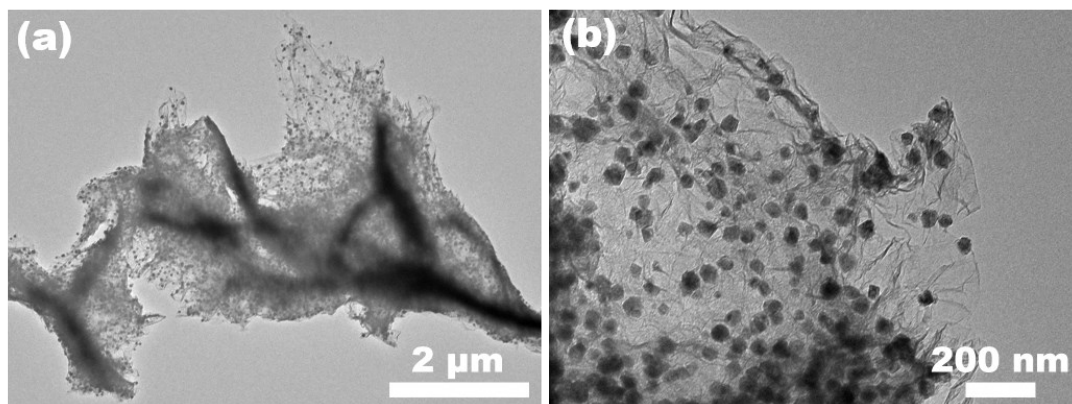


Fig. S3. TEM images of P-Fe₄N@NPG after 1 hour sonication.

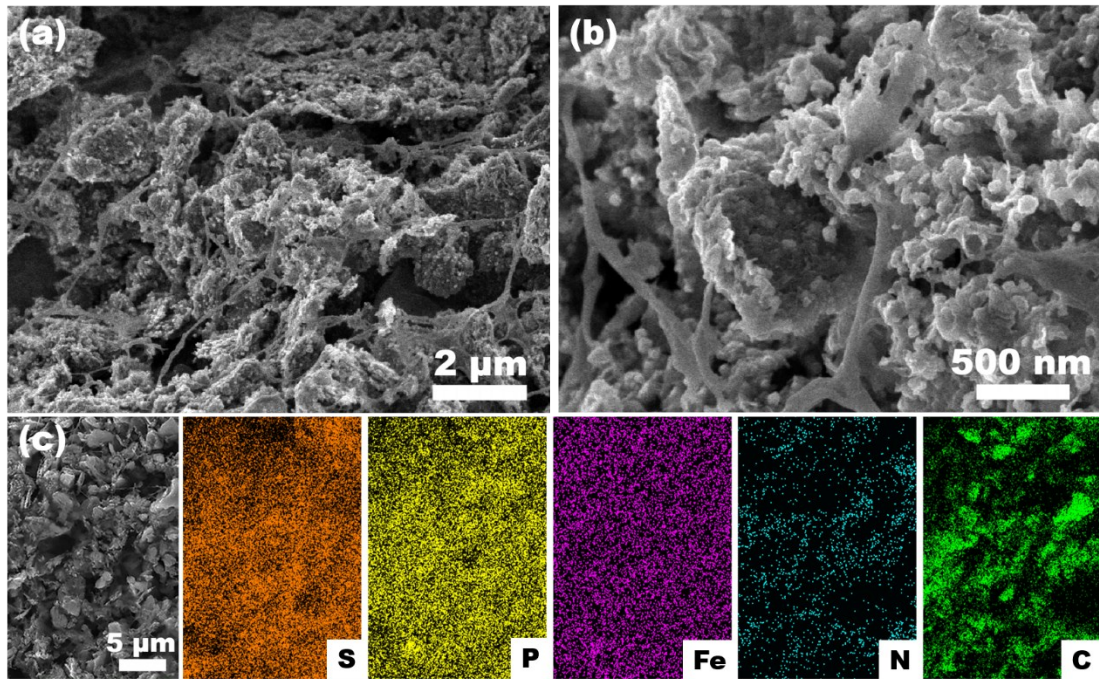


Fig. S4. (a, b) FESEM images and (c) The corresponding EDS elemental mapping images of the obtained P-Fe₄N@NPG/S composite.

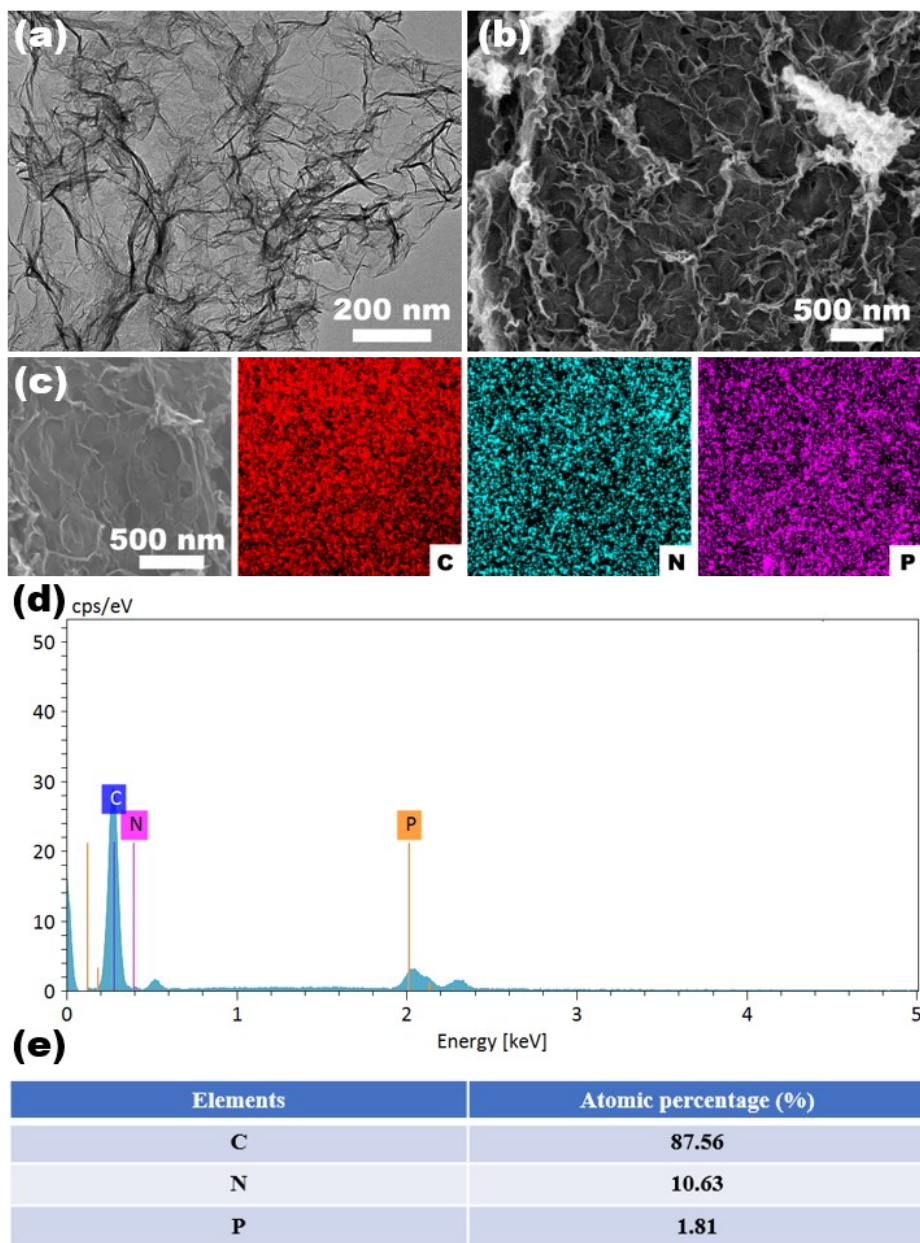


Fig. S5. (a) TEM and (b) FESEM images of NPG. (c) The corresponding EDS elemental mapping of NPG. (d) EDS spectrum and (e) percentage of elements of NPG.

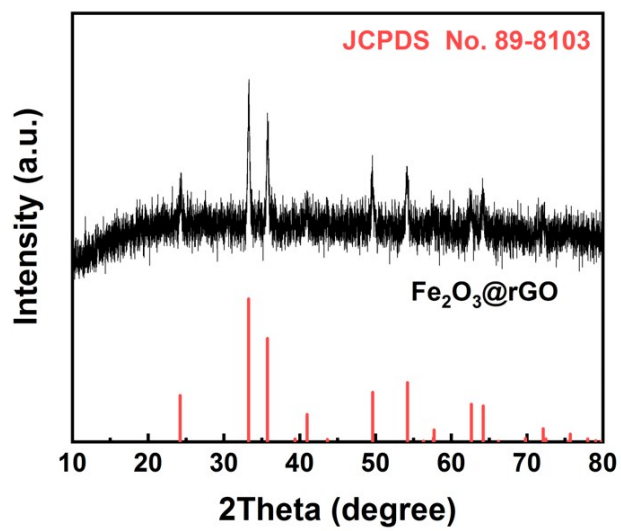


Fig. S6. The typical XRD pattern of the obtained Fe₂O₃@rGO.

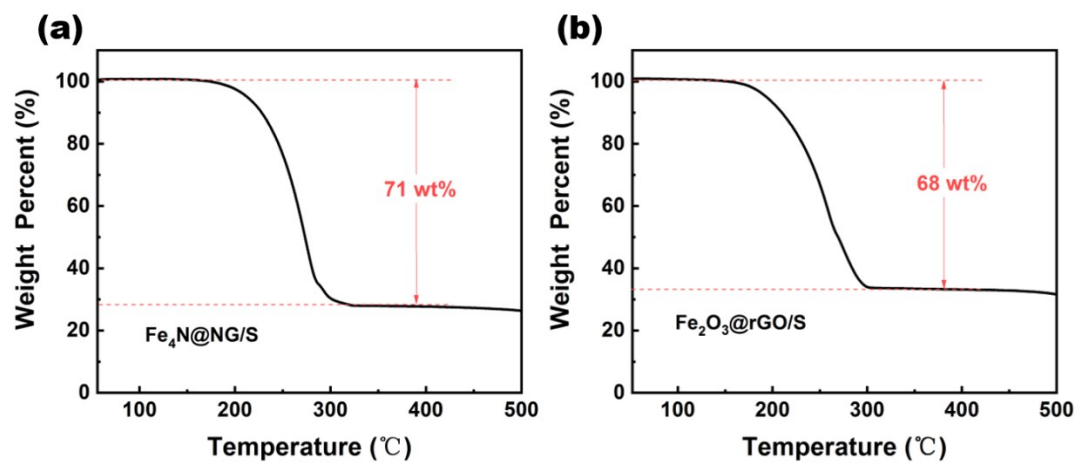


Fig. S7. TGA curves of (a) $\text{Fe}_4\text{N@NG/S}$ and (b) $\text{Fe}_2\text{O}_3@\text{rGO/S}$.

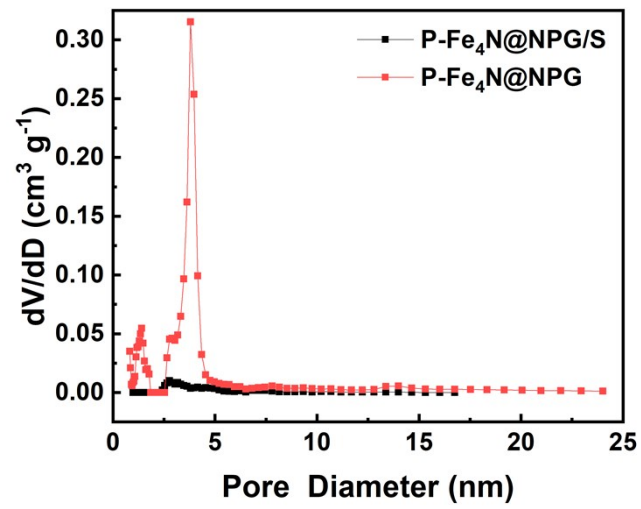


Fig. S8. Pore size distribution curves of P-Fe₄N@NPG and P-Fe₄N@NPG/S.

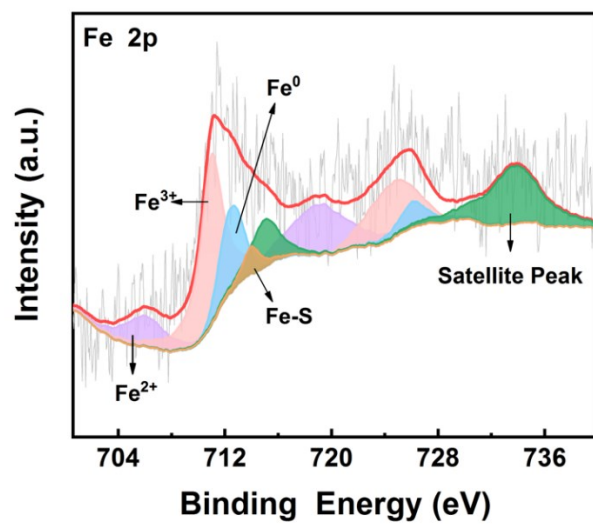


Fig. S9. XPS spectrum of the Fe 2p in full spectrum of P-Fe₄N@NPG after Li₂S₆ adsorption.

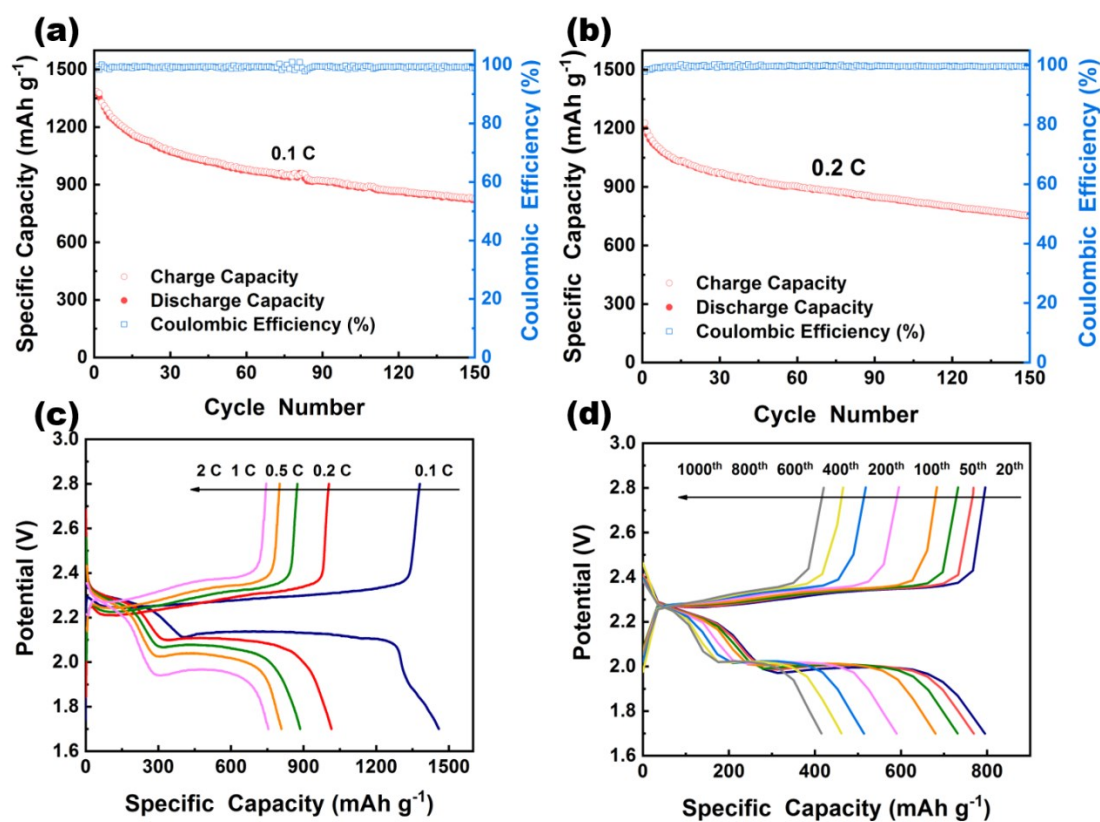


Fig. S10. (a, b) Cycling performances of P-Fe₄N@NPG/S cathode at 0.1 and 0.2 C, respectively. (c) Galvanostatic charge/discharge profiles of the P-Fe₄N@NPG/S cathode under different current densities. (d) Galvanostatic charge/discharge profiles of P-Fe₄N@NPG/S cathode at 1 C.

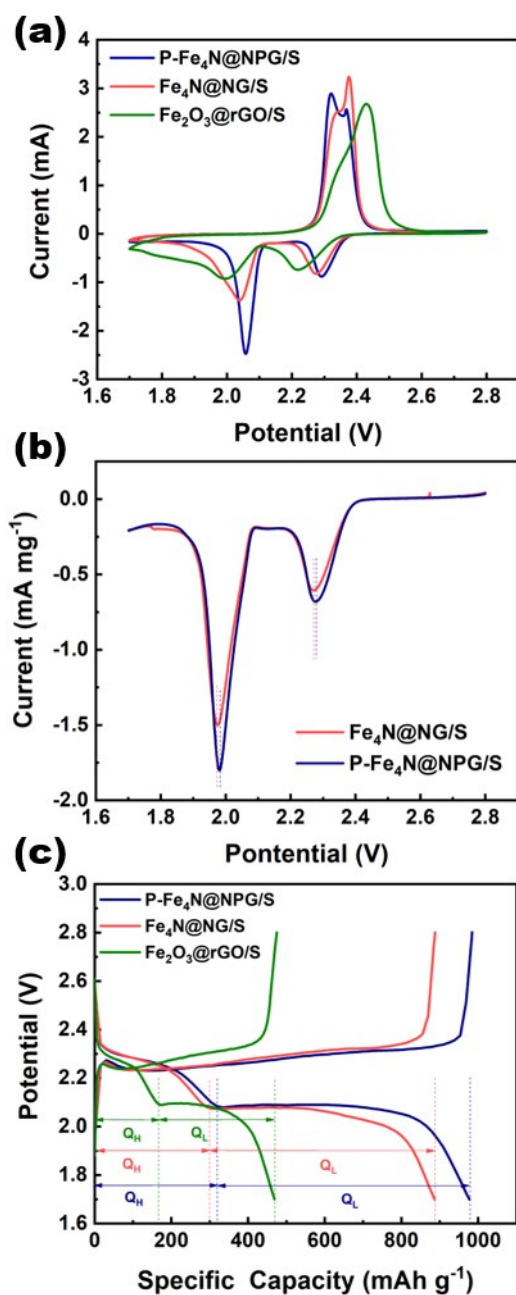


Fig. S11. (a) CV curves of P-Fe₄N@NPG/S, Fe₄N@NG/S and Fe₂O₃@rGO/S cathodes at scan rate of 0.1 mV s⁻¹. (b) The linear sweep voltammetry scanning curves. (c) Galvanostatic charge/discharge profiles of P-Fe₄N@NPG/S, Fe₄N@NG/S and Fe₂O₃@rGO/S cathodes at 0.5 C.

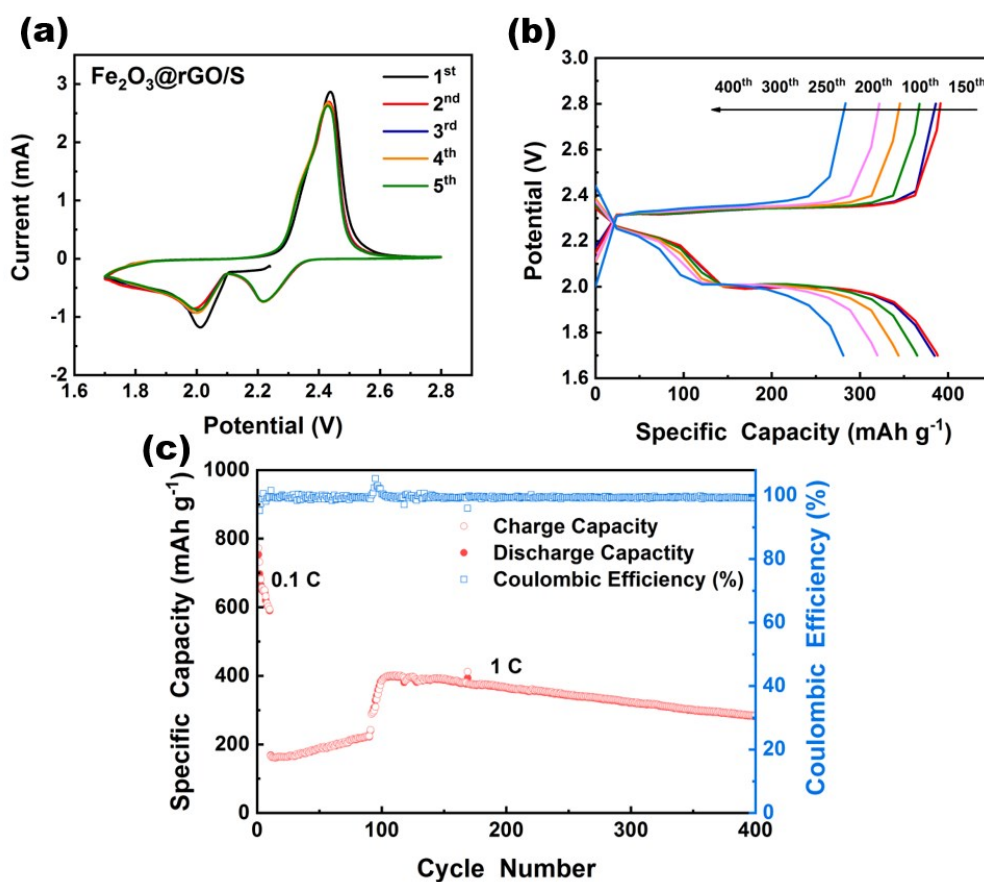


Fig. S12. The electrochemical performances of $\text{Fe}_2\text{O}_3@\text{rGO}/\text{S}$ cathode. (a) CV curves of $\text{Fe}_2\text{O}_3@\text{rGO}/\text{S}$ cathode at a scan rate of 0.1 mV s^{-1} . (b) Galvanostatic charge/discharge profiles and (c) Long-term cycling performance of $\text{Fe}_2\text{O}_3@\text{rGO}/\text{S}$ cathode at 1 C.

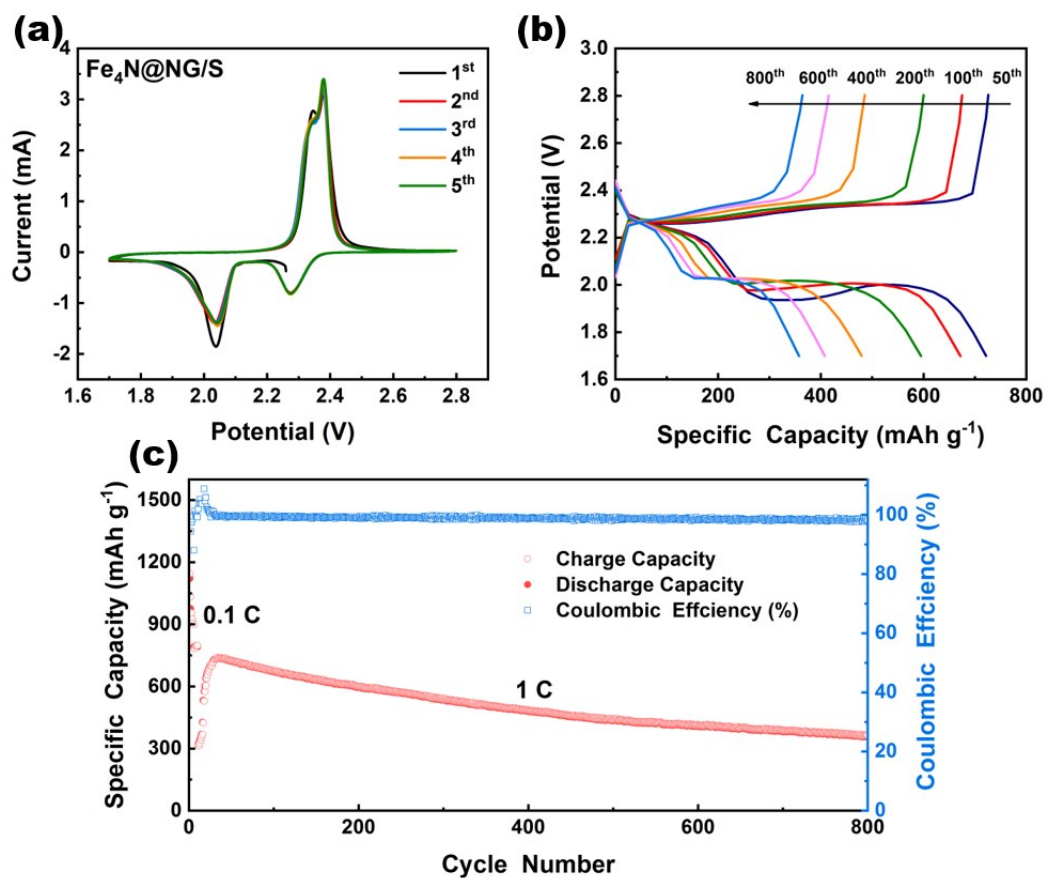


Fig. S13. The electrochemical performances of $\text{Fe}_4\text{N}@NG/S$ cathode. (a) CV curves of $\text{Fe}_4\text{N}@NG/S$ cathode at a scan rate of 0.1 mV s^{-1} . (b) Galvanostatic charge/discharge profiles and (c) Long-term cycling performance of $\text{Fe}_4\text{N}@NG/S$ cathode at 1 C.

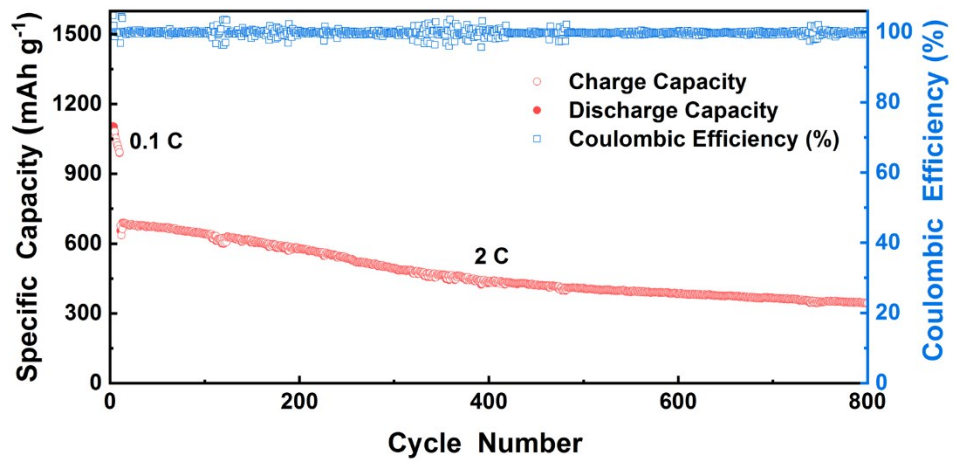


Fig. S14. Long-term cycling performance of P-Fe₄N@NPG/S cathode at 2 C.

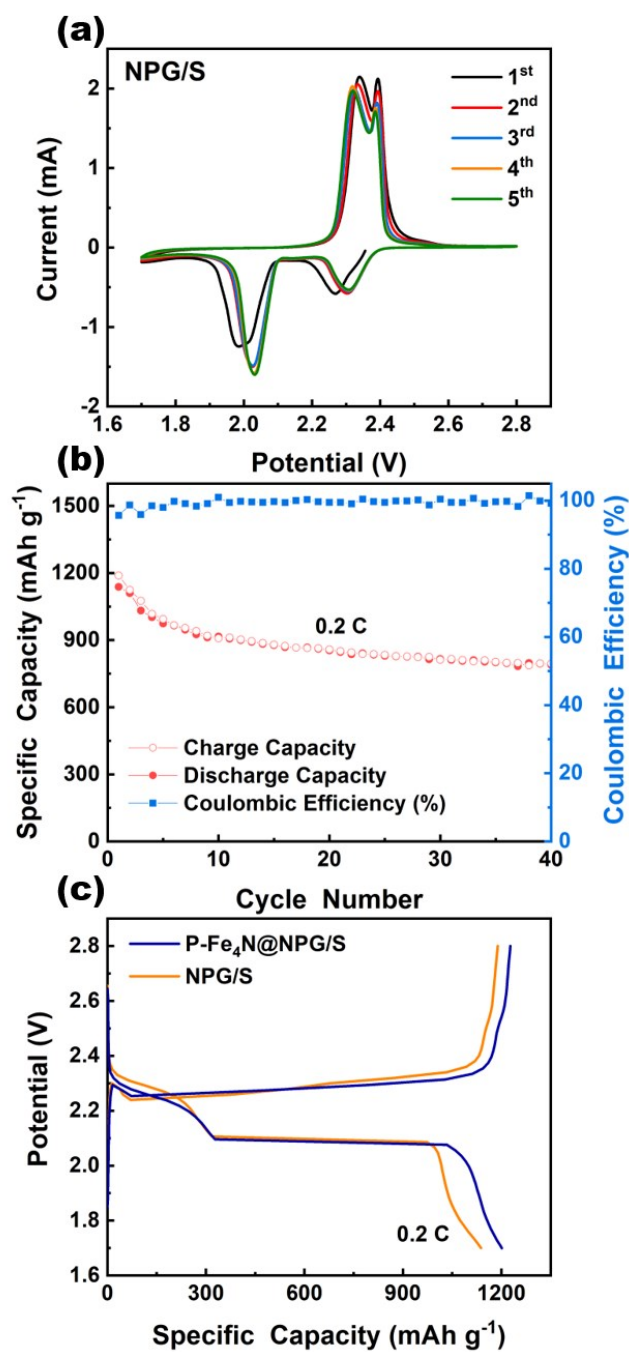


Fig. S15. (a) CV curves of NPG/S cathode at a scan rate of 0.1 mV s⁻¹. (b) Cycling performance and coulombic efficiency of NPG/S cathode at 0.2 C. (c) The typical galvanostatic charge/discharge voltage profiles of P-Fe₄N@NPG/S and NPG/S cathodes at 0.2 C.

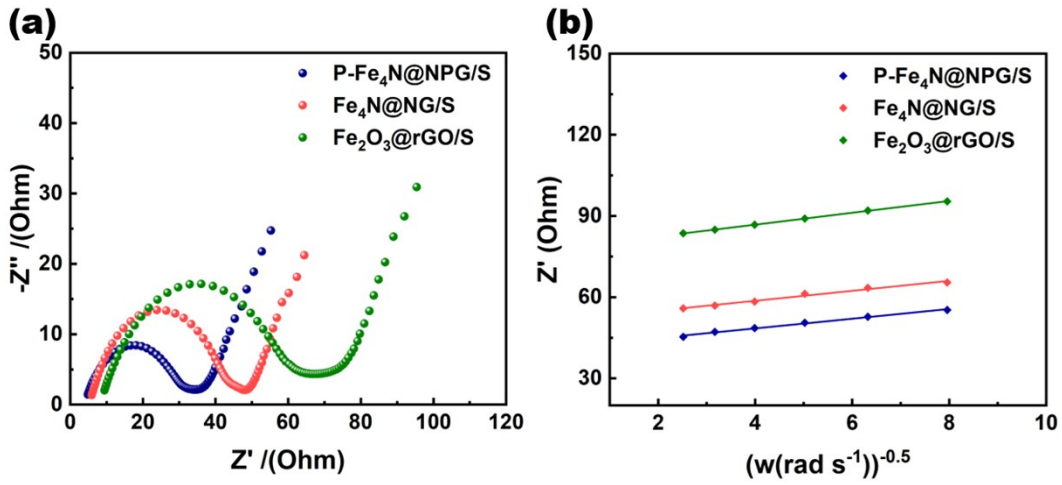


Fig. S16. (a) The electrochemical impedance spectra (EIS) of P-Fe₄N@NPG/S, Fe₄N@NG/S and Fe₂O₃@rGO/S cathodes before cycling. (b) The relationship between the Z' square root of angular frequency($\omega^{-0.5}$).

To further explore the reasons for the excellent performance and high conductivity of P-Fe₄N@NPG, we tested electrochemical impedance spectra (EIS) of P-Fe₄N@NPG/S, Fe₄N@NG/S and Fe₂O₃@rGO/S cathodes before cycling. The depressed semi-circle in the high-middle frequency region was attributed to the charge transfer resistance, and the slope part in the low frequency region was related with the ion diffusion process within the cathodes. The electrochemical impedance parameters were calculated according to the following equations (1-2).

$$Z_{re} = R_e + R_{ct} + \sigma\omega^{-0.5} \quad (1)$$

$$D_{Li^+} = 0.5(RT/AF^2C\sigma)^2 \quad (2)$$

In which the gas constant, angular frequency and the absolute temperature are expressed in terms of R , ω and T , while the electrode surface area, the Faraday constant, and molar concentration of Li^+ are denoted by A , F and C , respectively.

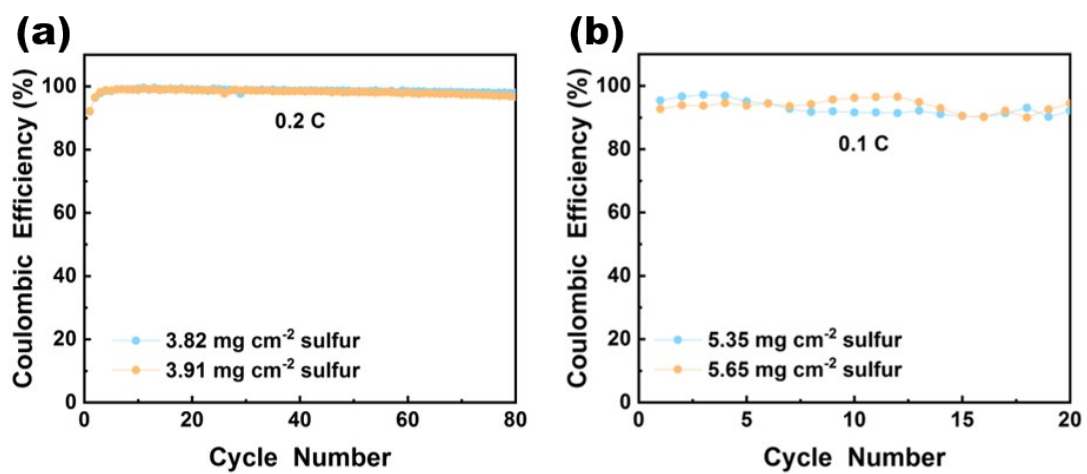


Fig. S17. (a, b) Coulombic efficiency of P-Fe₄N@NPG/S cathode of lean electrolyte at 0.2 C and 0.1 C, respectively.

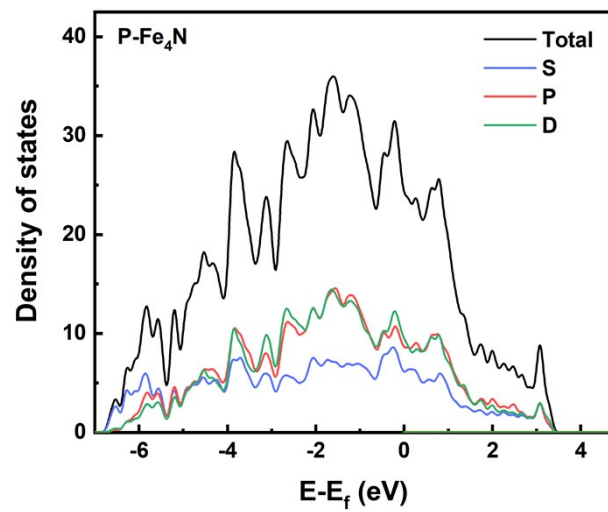


Fig. S18. Density of states of P-Fe₄N.

Table S1. The electrochemical performance of the obtained P-Fe₄N@NPG/S in this work compared with other similar materials reported in lithium-sulfur batteries.

Materials	Sulfur Content	Areal Mass of Cathode (mg cm ⁻²)	Current Rate	Cycle Number	Electrochemical Performance (mAh g ⁻¹)	Reference
TiN	58.8%	1.0	0.5 C	500	644	[1]
TiN	70%	1.4-1.7	1 C	300	505.2	[2]
MoN-VN	58.5%	1.13	1 C	500	555	[3]
WN	59%	0.92	2 C	500	358	[4]
Fe ₃ O ₄ -NC@ACC	54%	4.7	0.2 C	1000	760	[5]
CF/FeP@C		1.56	1 C	200	500	[6]
FeP/rGO/CNTs	75%	1.0	1 C	400	673	[7]
Fe-PNC/S	70%	1.3	0.5 C	300	557.4	[8]
N,S-Codoped Graphene	3.9 at. %	1.8-2.8	0.2 C	100	822	[9]
NPHPC	73%	0.88-1.59	1 C	200	575.1	[10]
P-Fe ₄ N@NPG	73%	1.1-1.4	1 C	1000	417.4	This Work

REFERENCE

- 1 Z. Cui, C. Zu, W. Zhou, A. Manthiram and J. B. Goodenough, *Adv. Mater.*, 2016, **28**, 6926-6931.
- 2 C. Li, J. Shi, L. Zhu, Y. Zhao, J. Lu and L. Xu, *Nano Res.*, 2018, **11**, 4302-4312.
- 3 C. Ye, Y. Jiao, H. Jin, A. D. Slattery, K. Davey, H. Wang, S-Z. Qiao, *Angew. Chem. Int. Ed.* 2018, **57**, 16703 –16707.
- 4 Z. D. Huang, Y. Fang, M. Yang, J. Yang, Y. Wang, Z. Wu, Q. Du, T. Masese, R. Liu, X. Yang, C. Qian, S. Jin and Y. Ma, *ACS Appl. Mater. Interfaces*, 2019, **11**, 20013-20021.
- 5 K. Lu, H. Zhang, S. Gao, H. Ma, J. Chen, Y. Cheng, *Adv. Funct. Mater.* 2019, **29**, 1807309.
- 6 J. Shen, X. Xu, J. Liu, Z. Liu, F. Li, R. Hu, J. Liu, X. Hou, Y. Feng, Y. Yu and M. Zhu, *ACS Nano*, 2019, **13**, 8986-8996.
- 7 S. Huang, Y. V. Lim, X. Zhang, Y. Wang, Y. Zheng, D. Kong, M. Ding, S. A. Yang and H. Y. Yang, *Nano Energy*, 2018, **51**, 340-348.
- 8 Z. Liu, L. Zhou, Q. Ge, R. Chen, M. Ni, W. Utetiwabo, X. Zhang and W. Yang, *ACS Appl. Mater.*

Interfaces, 2018, **10**, 19311-19317.

9 G. Zhou, E. Paek, G. S. Hwang and A. Manthiram, *Nat. Commun.*, 2015, **6**, 7760.

10 W. Ai, W. Zhou, Z. Du, Y. Chen, Z. Sun, C. Wu, C. Zou, C. Li, W. Huang and T. Yu, *Energy Storage Mater.*, 2017, **6**, 112-118.